NeuroImage: Clinical 22 (2019) 101754

Contents lists available at ScienceDirect

NeuroImage: Clinical

journal homepage: www.elsevier.com/locate/ynicl

Longitudinal analysis of structural changes following unilateral focused ultrasound thalamotomy

Francesco Sammartino[a], Fang-Cheng Yeh[b], Vibhor Krishna[a,*]

[a] Center for Neuromodulation, The Ohio State University, 480 Medical Center Dr., Columbus, OH 43210, USA
[b] Department of Neurological Surgery, University of Pittsburgh, PA, USA

ARTICLE INFO

Keywords:
Focused ultrasound
Thalamotomy
Tractography
Free water correction, Lesion characteristics

ABSTRACT

Objective: Focused ultrasound thalamotomy is an emerging treatment for essential tremor, and it is ideal for studying reorganization in the human brain after acute injury because it creates a controlled thalamic ablation without breaching the cortex. However, there is not yet a metric capable of detecting microstructural changes in the presence of acute phase edema with good sensitivity in the chronic phase, when the lesion boundaries become inconspicuous.

Methods: We prospectively studied microstructural changes at the lesion site using generalized q-sampling imaging with restricted diffusion imaging. We obtained diffusion-weighted MRI scans preoperatively, 1 day after (n = 18), and 1 year after (n = 9) focused ultrasound thalamotomy. The restricted diffusion imaging maps were compared at the group level, controlling for improvement in contralateral hand tremor.

Results: The restricted diffusion imaging metric significantly increased in the 1 day post images, and the area with restricted diffusivity extended beyond the lesion boundaries identified on T2-weighted imaging. Two distinct zones of microstructural changes were identified, and the lesion area was identifiable at 1 year. The anterior and medial aspects of the lesion had a significant changes in RDI at 1 year, potentially signifying re-organization. The voxels with significant changes in restricted diffusion imaging values extend beyond the VIM into the surrounding white matter.

Interpretation: Correcting for free water contamination with restricted diffusion imaging allowed us to study microstructural changes after focused ultrasound thalamotomy. We observed statistically significant changes in RDI in the anterior and medial aspect of the lesion at 1 year. Whether these changes represent tissue re-organization remains to be confirmed in future studies. These findings may support performing additional ablations antero-medially for durable efficacy.

1. Introduction

Focused ultrasound thalamotomy (FUS-T) was recently approved by the US FDA as an incisionless surgical treatment for patients with medically-refractory essential tremor (ET; (FDA, 2016). Contralateral hand tremor after FUS-T improves by approximately 50% (clinical rating scale for tremor [CRST]), and the results are sustained up to 24 months (Chang et al., 2018). Nonetheless, significant research is required to improve the reliability of clinical outcomes after FUS-T; e.g., up to 30% of patients lose efficacy after initial tremor reduction. The FUS-T lesion size can also be unpredictable and is often larger (Boutet et al., 2018; Krishna et al., 2018a) than the reported lesion size after radiofrequency thalamotomy (Hirai et al., 1983). Interestingly, these lesions eventually become indistinguishable from the surrounding region a few months after FUS-T, despite sustained efficacy (Elias et al., 2013a). The inherent complexity of the physics governing ultrasound energy transfer to biological tissues may be responsible for some of the differences in lesion shapes and sizes, compared with conventional radiofrequency thalamotomy and gamma-knife lesioning (Elias et al., 2013b). In addition, the relatively low resolution of intraoperative

Abbreviations: dMRI, diffusion MRI; RDI, Restricted Diffusion Imaging; FA, Fractional Anisotropy; AD, Axial Diffusivity; RD, Radial Diffusivity; MD, Mean Diffusivity; TFCE, Threshold-Free Cluster Enhancement; QSDR, q-space diffeomorphic reconstruction algorithm; ANTs, Advanced Normalization Tools; FUS-T, Focused Ultrasound thalamotomy; SDF, spin diffusivity function; NQA, normalized quantitative anisotropy; ODF, orientation distribution function; ET, Essential Tremor; DTI, Diffusion Tensor Imaging; DWI, Diffusion-weighted imaging; ROC, Receiver operator characteristics

* Corresponding author at: Center for Neuromodulation, Department of Neurosurgery & Department of Neuroscience, The Ohio State University, 480 Medical Center Drive, Columbus, OH 43210, USA.
E-mail address: vibhorkrishna@yahoo.com (V. Krishna).

https://doi.org/10.1016/j.nicl.2019.101754
Received 22 October 2018; Received in revised form 13 January 2019; Accepted 9 March 2019
Available online 12 March 2019

thermometry imaging, coupled with an incomplete understanding of the thermal dose response from repeated ultrasound ablations (or sonications) at the same focal point, further complicates this picture (Chen et al., 1997). For instance, the temperature estimation with MR thermography is indirect and based on the proton shift from a baseline image to compute a thermal map of the area. The Exablate 4000 transducer (Insightec Inc.) obtains 2-D thermography images with an in-plane resolution of 4 mm, which only allows for a limited estimation of the lesion size and shape. It is reasonable to expect that some of these issues may be addressed with technological advancement in the transducer design (e.g., the incorporation of a head coil for volumetric thermometry acquisition) and with the maturation of the learning curve in the surgical techniques using this novel technology (The reference for this has been provisionally accepted. can you please advise how to reference it here). However, a better understanding of the in vivo tissue changes at the lesion site, and their evolution in the long term, will be critical for improving the ablation technique and discovering the mechanisms underlying eventual loss of efficacy after FUS-T.

Histologically, FUS lesions include two zones and the surrounding edema: zone 1 represents the central coagulative necrosis and the surrounding zone 2 includes tissue disruption and apoptosis (Elias et al., 2013c). Although these zones have been approximated with the T2 hypointensity (zone 1) and hyperintensity (zone 2) on MRI (Elias et al., 2013c), such organization could not be replicated in imaging studies because the conventional diffusion metrics become less reliable in detecting changes in tissue microstructure in the presence of significant tissue edema and cellular infiltration immediately post-FUS-T, and cannot detect discrete lesions in images beyond three months (Fig. 1). Therefore, novel methods are required to understand structural reorganization in the brain after FUS-T to explore the causes of reduced efficacy and potentially refine the surgical technique.

Diffusion MRI (dMRI) is increasingly being used to study white matter pathways in vivo, but the conventional diffusion tensor imaging approach (Basser, 1995) has limited sensitivity and specificity to neurodegenerative disorders due to the simplicity of the tensor model (Ito et al., 2007). Here, we used a model-free approach called generalized q-sampling imaging (GQI) to address these limitations (Yeh et al., 2010). This algorithm accounts for free water molecules during estimation of the spin diffusivity function (SDF) at each voxel, without assuming a pre-existing diffusion model. Here, 'free water' refers to water molecules that diffuse without being restricted by the cellular environment. There is evidence from previous reports that free water, although estimated using a different tensor modeling scheme, may directly correlate with the proportion of extracellular space (Pasternak et al., 2012). While GQI has been shown to be effective in correcting this free water effect (Zhang et al., 2013), the restricted diffusion imaging metric (RDI; (Yeh et al., 2017) is a model-free approach that estimates the density of diffusing spins with respect to their diffusion displacement, thereby eliminating non-restricted diffusion. This metric was shown in mice myocardium to directly correlate with increased cell density in histology due to neutrophils infiltration. In addition, this metric produced more consistent results when compared to other diffusion MR metrics that are based on the tensor model, such as apparent diffusion coefficient and mean diffusivity, which may become uninterpretable in the presence of edema and cellular infiltration. In this study, we used RDI to study microstructural changes in the brains of patients undergoing FUS-T. We examined three hypotheses: i) RDI increases at the lesion site 1 day after FUS-T, and can distinguish between the two zones of microstructural change at the lesion site; ii) RDI changes can be detected 1 year after FUS-T; iii) RDI can distinguish clinically relevant changes (e.g., ideal lesion size for efficacy) both in the vicinity of and away from the lesion site. We tested these hypotheses in a prospective cohort of ET patients who underwent unilateral FUS-T and dMRI at baseline, 1 day post (n = 18), and 1 year post-FUS-T (n = 9).

2. Materials and methods

2.1. Patient demographics and clinical information

Eighteen patients participated in the study from 2014 to 2018 and provided written informed consent as a part of this IRB-approved study. All patients were diagnosed with ET by a multidisciplinary team.

2.2. Surgical treatment

Details of the surgical procedure for FUS-T have been previously described in a separate report (Krishna et al., 2018a). Briefly, the ventral intermediate nucleus (VIM) of the thalamus was targeted using a tractography-based approach (Sammartino et al., 2016). An average of 13 sonications were performed until we reached a target temperature of 55 °C and an accompanying contralateral hand tremor suppression of > 50% from baseline.

2.3. dMRI acquisition

Diffusion-weighted images were acquired on a 3T MRI scanner (Achieva, Philips Medical Systems) using a 32-channel head coil. The Philips 3T used in the present study met routine quality assurance. Whole-brain diffusion imaging data were acquired using a single-shot spin echo EPI sequence, consisting of the following parameters: repetition time = 8100 ms, echo time = 68 ms, flip angle = 90°, diffusion gradient (monopolar) directions = 59, diffusion gradient timing DELTA/delta = 32.8 / 21.6 ms, b-values: 0, 1000 s/mm^2, fat suppression using SPIR, field of view = 240 × 240 mm, in-plane resolution = 2 mm isotropic, number of transverse interleaved slices = 60, zero gap, slice thickness = 2 mm, SENSE factor = 2.

2.4. Structural brain imaging acquisition

As standard of care, we also acquired a 3D fast gradient echo T1-weighted (T1W) sequence with the following parameters: repetition time = 8.2 ms, echo time = 3.7 ms, flip angle = 8°, field of view = 240 mm^2, acquisition matrix = 240 × 240, voxel size = 1 mm isotropic (n = 160, transverse), SENSE factor = 1.5. A 3D whole-brain axial T2 at 1 mm resolution was acquired to aid in the evaluation of lesion boundaries and for dMRI registration (TE 80 ms, TR 6650 ms, 0.83 × 0.83 × 1.2 mm, flip angle = 90°).

2.5. Lesion segmentation and group structural template creation

Each thalamic lesion was manually segmented on the 1 day post-operative T2-weighted (T2W) imaging using ITK-snap software by a fellowship-trained neurosurgeon (FS). A label was then created to include the necrotic center and the rim immediately surrounding it. Each mask was then dilated by two voxels to include the tissue with edema infiltration around the second lesion 'ring'. T1W and T2W images were then registered to MNI T1W 2009c template space using a combination of linear and nonlinear transforms (FSL FLIRT and FNIRT; (Jenkinson et al., 2012). The corresponding transform was applied to each lesion, using nearest-neighbor interpolation. The MNI aligned 1-day post-surgery T2W images were averaged to create a group template.

2.6. Longitudinal analysis of RDI changes

Data preprocessing was mainly performed using TORTOISE (https://science.nichd.nih.gov/confluence/display/nihpd/TORTOISE) and DSISTUDIO software (https://github.com/frankyeh/DSI-Studio) interfaced with custom R scripts. An overview of the processing pipeline is given in Fig. 2.

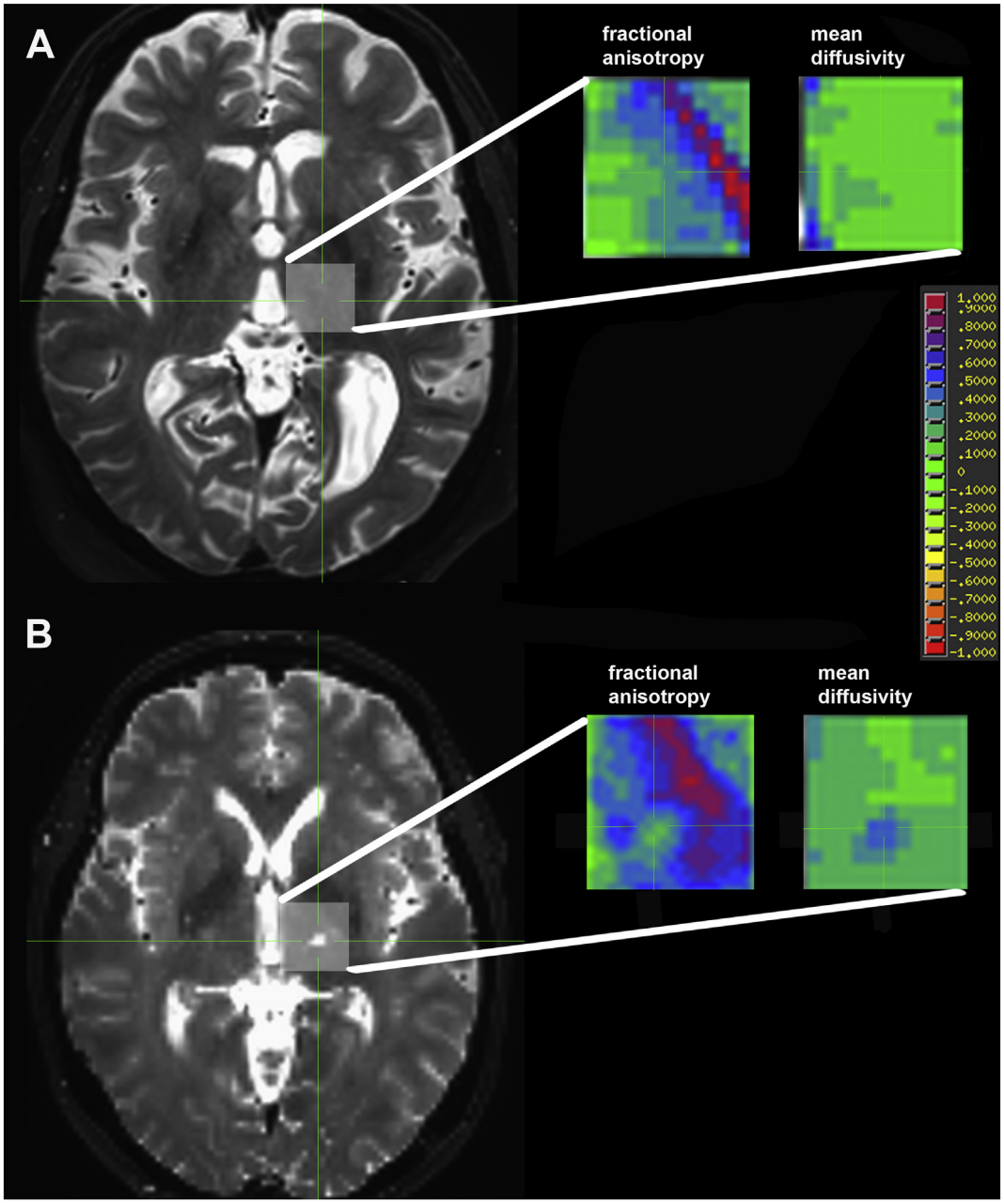

Fig. 1. (A) Lesion boundaries become inconspicuous after FUS-T in contrast to radiofrequency thalamotomy (B). The structural T2-weighted images are compared between a patient with left radiofrequency thalamotomy (imaging obtained 18 years after surgery) and a patient (B) who had focused ultrasound thalamotomy (imaging obtained 1 year after surgery) for the treatment of essential tremor. In contrast to the radiofrequency lesion, both fractional anisotropy (FA) and mean diffusivity (MD) maps in the corresponding location fail to reveal the FUS-T lesion.

2.7. Diffusion preprocessing and determination of imaging quality

Each diffusion scan was first corrected for distortions due to eddy currents and head motion as implemented in the software TORTOISE (Pierpaoli et al., 2010). Briefly, we first computed the transformation for motion and eddy distortion correction and the appropriate reorientation of the b-matrix of each image to the new coordinate system (Rohde et al., 2004). Then, the first non-diffusion-weighted (b = 0 s/mm^2) image of each DTI dataset was registered (affine transform) to the T2W structural image of the same subject. We then applied these transforms simultaneously to the DWI images to produce the raw corrected DWIs used in the analysis.

2.8. QSDR reconstruction and estimation of RDI in common space

For each subject, the motion-corrected diffusion data were reconstructed in a common stereotaxic space (MNI ICBM 2009c Nonlinear Asymmetric 1 mm) using the q-space diffeomorphic reconstruction (QSDR) algorithm (Yeh and Tseng, 2011); the goodness-of-fit between the warped image and template image was evaluated using the R^2 coefficient. All patients in the study had an R^2 coefficient > 0.72; we used a diffusion sampling ratio parameter value of 1.25.

Whole-brain RDI maps were extracted for each time point. Each map was masked with the lesion label. In a subsequent analysis, each RDI map was masked using a cubic label map (AfNI 3dcalc software) of ten slices, centered on the necrotic center of the lesion, to study the longitudinal changes in the lesion neighborhood. Finally, the RDI maps

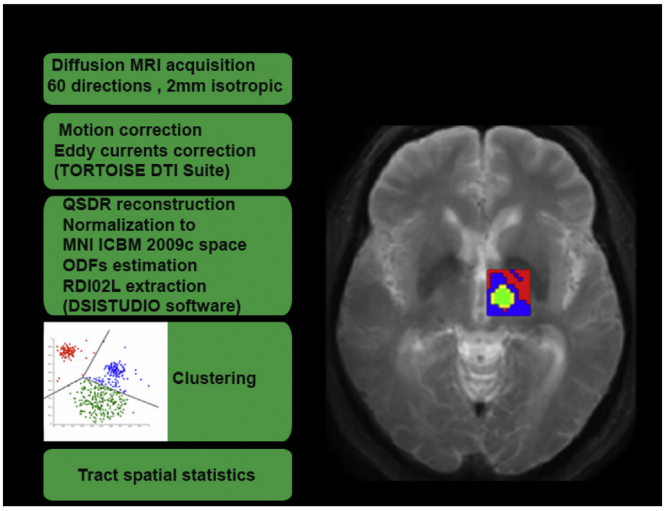

Fig. 2. Processing pipeline: flow chart that illustrates the steps of the dMRI processing pipeline from acquisition to statistical analysis.

were masked using a mask comprising the left hemisphere plus the right and left cerebellum to study changes in the long-range white matter pathways afferent/efferent to the thalamic ventro-lateral nuclei group. RDI maps were thresholded with a lower threshold of 0.8 to exclude the cortical ribbon from the analysis, and masked using the white matter segmentation map in template space, distributed with AfNI SUMA software (Saad et al., 2004). Across subjects, the average center of mass (COM) coordinates for the group lesion were x = −13.83, y = −18.18, and z = −2.43 (all lesions were on the left thalamus).

2.9. Unsupervised clustering of RDI changes

Maps of the voxel-wise percentage of RDI change at the slab level were computed for the following comparisons: baseline vs. 1 day post (18 comparisons); 1 day vs. 1 year post (9 comparisons). Using the NbClust library in R (Charrad et al., 2014), the optimal number of clusters was estimated based on the lower value of the sum of squared Euclidean distances from the center. This number resulted in four zones in both comparisons. At this point, a K-means algorithm implementation with 5000 random initializations was used to cluster the maps at the single-patient level.

We performed tractography using DSISTUDIO software on the nine patients that had 1 year imaging data. For each baseline (pre-surgery) and 1 year scan, we seeded from zones 1 and 2 (the group-level union mask for each zone) using the left precentral gyrus and the right cerebellum as 'end' masks (MNI structural atlas). Fiber tracking was initiated by randomly seeding the region of interest and using all directions of ODFs per voxel. Fiber progression continued with a step size of 1 mm, a minimum fiber length of 2 mm (max 200 mm), and a turning angle threshold of 90°. No tract smoothing was used. Tracking terminated when the relative normalized-QA for the incoming direction dropped below a threshold of 0.02 or a limit of 500,000 seeds was reached. We then saved the tractography maps and totaled the number of streamlines.

2.10. Estimation and comparison of FA, MD, RD, AD maps

Maps of fractional anisotropy (FA), mean diffusivity (MD), radial diffusivity (RD), and axial diffusivity (AD) were computed at the slab level (FSL DTIFIT; (Burzynska et al., 2010), nonlinearly registered to the template (MNI ICBM 2009c Nonlinear Asymmetric 1 mm) using a combination of linear and diffeomorphic (SyN) registration with nearest-neighbor interpolation (ANTs software; (Avants et al., 2009), and used to compare the baseline and 1 day post time points.

2.11. Statistical analysis

We analyzed the 'raw' RDI maps in general linear models (Glm, FSL) with F-tests to test for differences across time points, followed by *t*-tests to understand the direction of the significant RDI changes, controlling for contralateral hand tremor improvement. The tests were run through randomise (FSL suite) software with threshold-free cluster enhancement (TFCE; (Smith and Nichols, 2009), using 5000 permutations for the baseline vs. 1 day comparison ($n = 18$) and 256 'exhaustive' permutations for the 1 day vs. 1 year comparison. We scaled and centered the median 'percent tremor improvement' variable before adding into the Glm.

The FA, MD, RD, and AD maps were compared with a t-test using 5000 permutations through randomise with TFCE. Receiver operator characteristic (ROC) curves were computed using lesion size and percentage of tremor improvement (3 months) as outcome variables (R library pROC; (Robin et al., 2011).

Data availability statement: The data that support the findings of this study are available from the corresponding author upon reasonable request.

3. Results

3.1. Demographic and clinical information

The mean age was 73.4 years (SD: 8.88); seven patients were women. Patients had a mean of 61.36% contralateral hand tremor improvement at 3 months after treatment (SD 22.46), with a sustained benefit seen in the nine patients who completed the follow up at 1 year (percentage of improvement from baseline; mean: 57.87; SD: 13.45; Supplementary Table 1).

3.2. Metrics comparison at the slab level

RDI showed voxels largely overlapping with the group lesion in the baseline vs. 1 day post comparison ($p < 0.05$). The other metrics tested were either significant in two voxels located at the medial border of the lesion(FA & MD), or not significant (RD: not significant [$p = 0.23$] - AD: not significant [$p = 0.25$]; Fig. 3).

3.3. RDI after FUS-T: two distinct zones

RDI values uniformly increased in the lesion area in all patients at 1 day post (18 subjects, $p < 0.001$). At the group level, the mean RDI increased by 54.57% (SD 28.43). Using unsupervised clustering, we identified two concentric zones at the lesion site: zone 1 (RDI median increase: 56.8; SD 25.6) and zone 2 (RDI median increase: 48.4; SD 29.6; Fig. 4). Zones 1 & 2 extended beyond the hyper and hypointense lesion rings identified on T2W imaging. Another cluster (zone 3), corresponding with edema on T2 imaging, was also identified. Fig. 4b shows the density distribution of the percentage of RDI change in each zone at the group level. The difference between RDI in zone 1 and zone 2, and between zone 1 and zone 3, was statistically significant (*t*-test, $p < 0.01$). At 1 day post-procedure, the lesion label map from the T2 scan overlapped with 84.65% (SD 9.73) of zone 1 and 60.95% (SD 14.69) of zone 2. These finding support the observation that both zones are part of the lesion seen acutely on T2. The number of streamline counts significantly ($p < 0.001$) decreased in Zone 1 at 1year (mean & SD streamline counts; baseline: 166293& 52355, 1 year: 80997 & 20117). The streamline count decrease in Zone 2 was not statistically significant (Fig. 5).

3.4. RDI changes can be detected even at 1 year post-FUS-T

After the initial increase at 1 day post, RDI decreased significantly at 1 year post-FUS-T (Fig. 4). The median RDI at the lesion site decreased

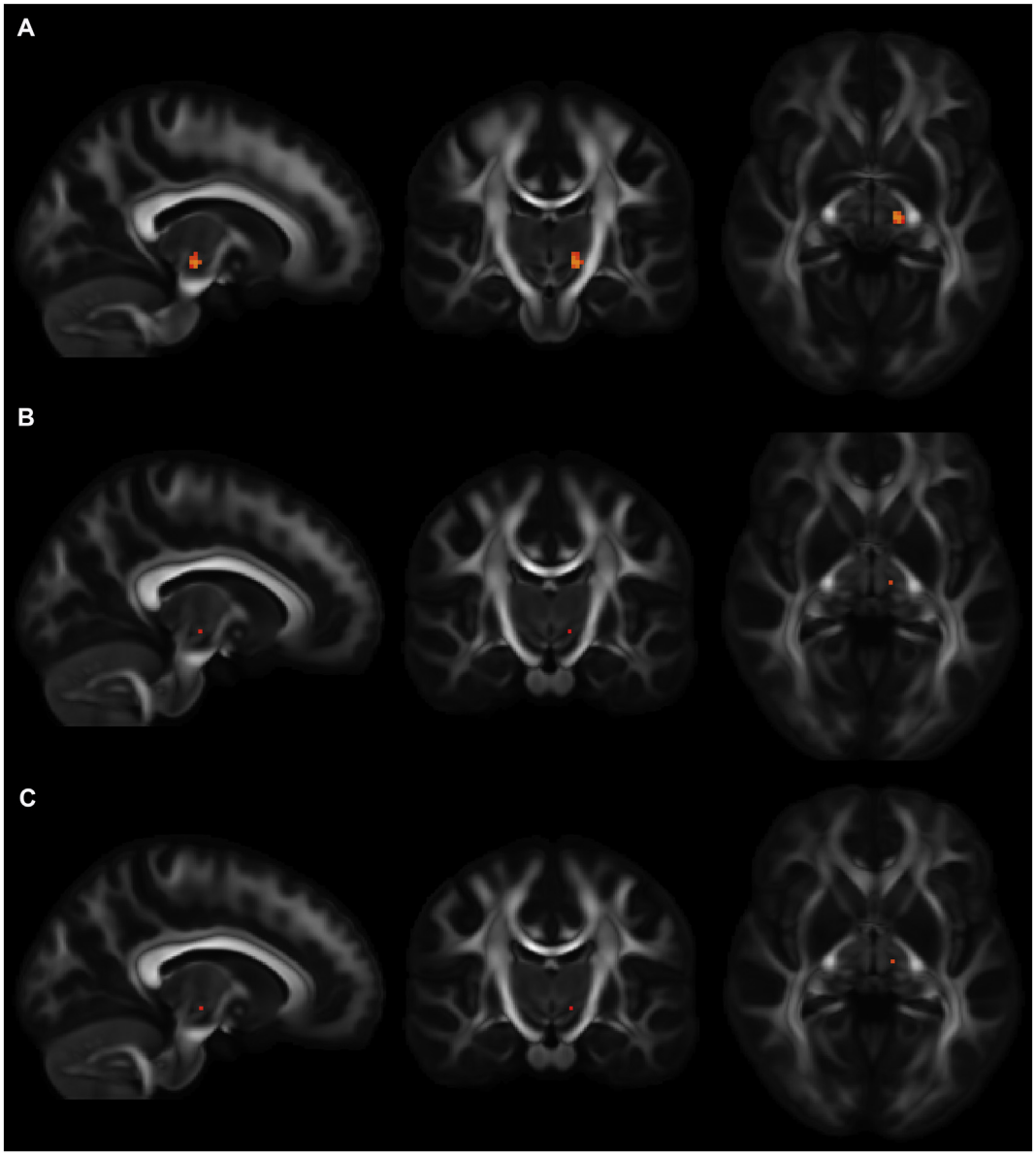

Fig. 3. Group-level comparison of diffusion metrics at the slab level: Thresholded maps resulting from the *t*-test (FSL randomise, 5000 permutations with TFCE), comparing baseline and 1 day post values. From the top: RDI (A), FA (B), MD (C) comparison maps (threshold $p < 0.05$).

between 1 day post and 1 year post-FUS-T by 25% (SD 12.83; $p < 0.01$). The comparison between 1 day post and 1 year post showed a significant difference between zone 1 and zone 2 (*t*-test; $p < 0.01$) after clustering. Although the median RDI in zone 1 decreased by 17.80% (SD 11.87), the median RDI decrease in zone 2 was more pronounced (38.26%; SD 11.13). Interestingly, the lesion could still be identified in the 1 year post imaging, even in the absence of clear T2 hypointensity (Fig. 6C). This area corresponded with zone 1 in 1 day post imaging, after clustering.

3.5. Clinically relevant microstructural changes based on RDI

To ascertain the absolute RDI value within the FUS-T 'lesion', we first identified voxels with a significant increase in RDI at 1 day post-FUS-T across all patients (Fig. 7A). These voxels have an 86% overlap with the T2 hyperintense lesion epicenter and a mean volume of 152 cubic mm. The median RDI value in this zone was 2.80 (SD 0.98), which was a significant increase from 1.66 (SD 0.69) at baseline.

Next, we explored the ideal lesion size and location for tremor improvement. This analysis was performed separately for tremor improvement at 3 months and 1 year. Voxels with significant RDI increase, controlling for tremor improvement, at 3 months are shown in Fig. 7B. The group-level lesion was centered on the lesion epicenter, but also extended into the dorsal thalamus and the subthalamic area. The volume of these significant voxels was 456 cubic mm. The median RDI value in these voxels was 1.78 (SD 0.52) at baseline and increased to 2.83 (SD 0.25) at 1 day post. As shown in Fig. 7C, the voxels with significant RDI decrease at 1 year were significantly smaller and overlapped with the lesion epicenter, but also incorporated surrounding voxels, especially below the thalamus.

3.6. Microstructural reorganization around the lesion at 1 year

To study regions with significant reorganization after FUS-T, we used *t*-tests to compare 1 day post and 1 year post images after adjusting for the percentage of tremor improvement. The surviving voxels ($p < 0.05$) are shown in Fig. 7D. A significant decrease in RDI was observed around the lesion epicenter, especially in the medial and

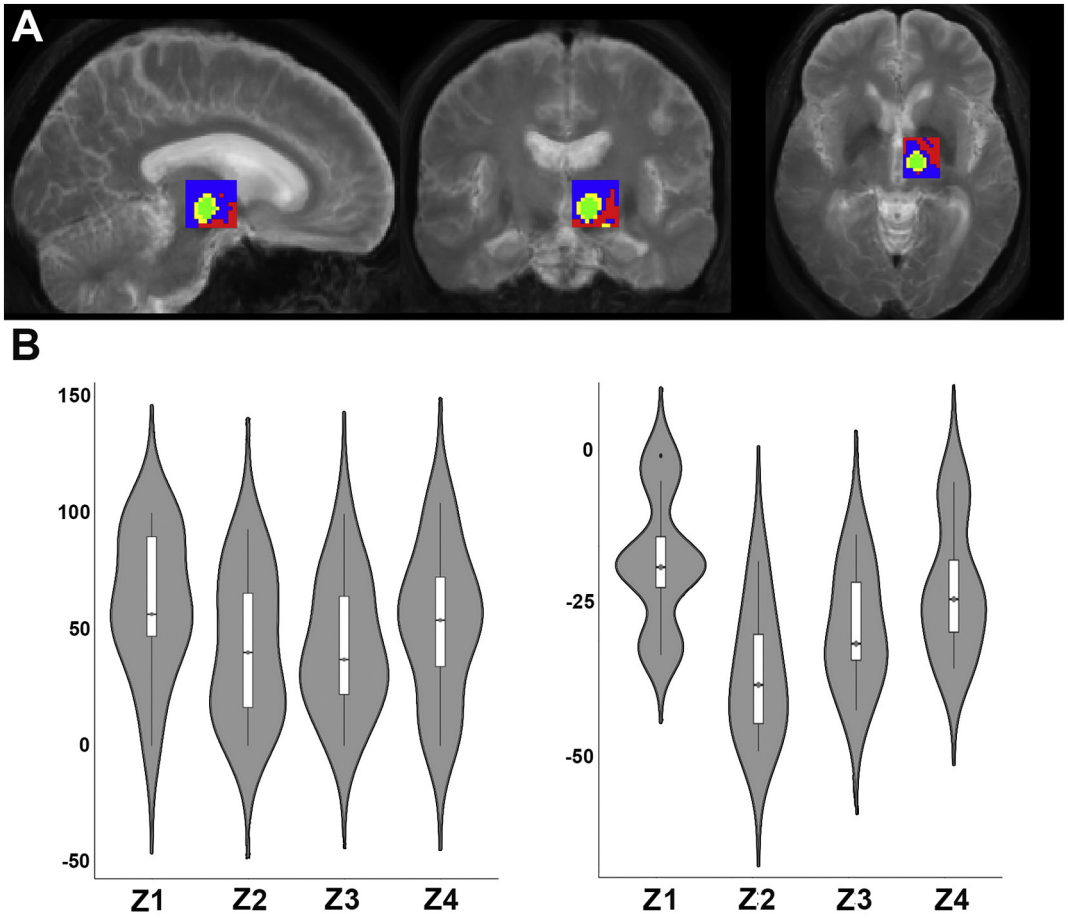

Fig. 4. The different zones resulting from RDI clustering. (A) Green: zone 1; Yellow: zone 2; Blue: zone 3; Red: zone 4. (B) Violin plots for the group level RDI percentage changes in each zone, between baseline and 1 day post, and between 1 day and 1 year post maps. (For interpretation of the references to color in this figure legend, the reader is referred to the web version of this article.)

anterior aspects of it.

3.7. Specificity and sensitivity in the prediction of lesion size and tremor improvement

We used empirical ROC curves to examine the sensitivity and specificity at all possible cutoffs of lesion size and percentage of tremor improvement at 3 months post. The median lesion size was 283 cubic mm (SD 190.01), and the median tremor improvement was 64.58% (SD 22.46). The analysis of ROC curves showed that the volume of the final lesion in T2W imaging can be predicted by normalized RDI change at the lesion site. RDI is scaled by the maximum spin density, which is why we scaled the values by the contralateral tissue for comparison (inverted mask x-coordinate, area with no lesion). The area under the ROC curve was 0.889 (95% confidence interval: 0.74–1), but it was 0.617 when the same metric was used to predict the percentage of tremor improvement. FA showed suboptimal results (Supplementary Fig. 1).

4. Discussion

In this study, we investigated the longitudinal microstructural changes associated with unilateral thalamotomy after FUS-T in a prospective cohort. We show that (i) it is feasible to study microstructural changes in the thalamotomy lesion neighborhood after removal of the signal due to free water diffusion, thus allowing the study of changes in regions with edema or degeneration; (ii) RDI increases immediately after FUS-T and can be clustered in two concentric zones of microstructural changes; and (iii) RDI changes can be detected even one year after FUS-T.

Focused ultrasound thalamotomy is a novel surgical option for patients with medication-resistant ET (FDA, 2016). The first reports of FUS ablation procedures date back to the work of William J. Fry in the 1950s (Fry et al., 1954; Harary et al., 2018b). At that time, the necessity of performing a craniotomy to target the basal ganglia with ultrasound beams and the lack of lesion control, coupled with the rise of deep brain stimulation, lead clinicians to abandon this technology. FUS technology was revived nearly 40 years later with the introduction of phased arrays and phase correction algorithms to overcome the need to open the skull. Finally, the refinement of MR thermography for lesion monitoring allowed the real-time estimation of the location and temperature at the focal point (Kennedy et al., 2003). Consequently, FUS-T is now performed with triple monitoring: clinical, thermography, and anatomical (Krishna et al., 2018b). In the only large, multi-institutional randomized trial, ET patients experienced a 47% tremor reduction at 3 months, with approximately 60% of patients showing 40% or greater improvement in contralateral hand scores (CRST A; (Elias et al., 2016)). However, not all patients experience similar tremor reduction, and about one third eventually lose their initial tremor improvement. Although tractography-based VIM targeting offers some additional improvement (blinded three-month improvement of 57%;(Krishna et al., 2018a), these results are still inferior to conventional thalamotomy (Schuurman et al., 2000) and deep brain stimulation (DBS; the current standard of care), where the acceptable tremor improvement can be approximately 70% at 12 months (Hariz et al., 2002). There is an urgent need to study the predictors of good outcomes, especially those associated with lesion characteristics.

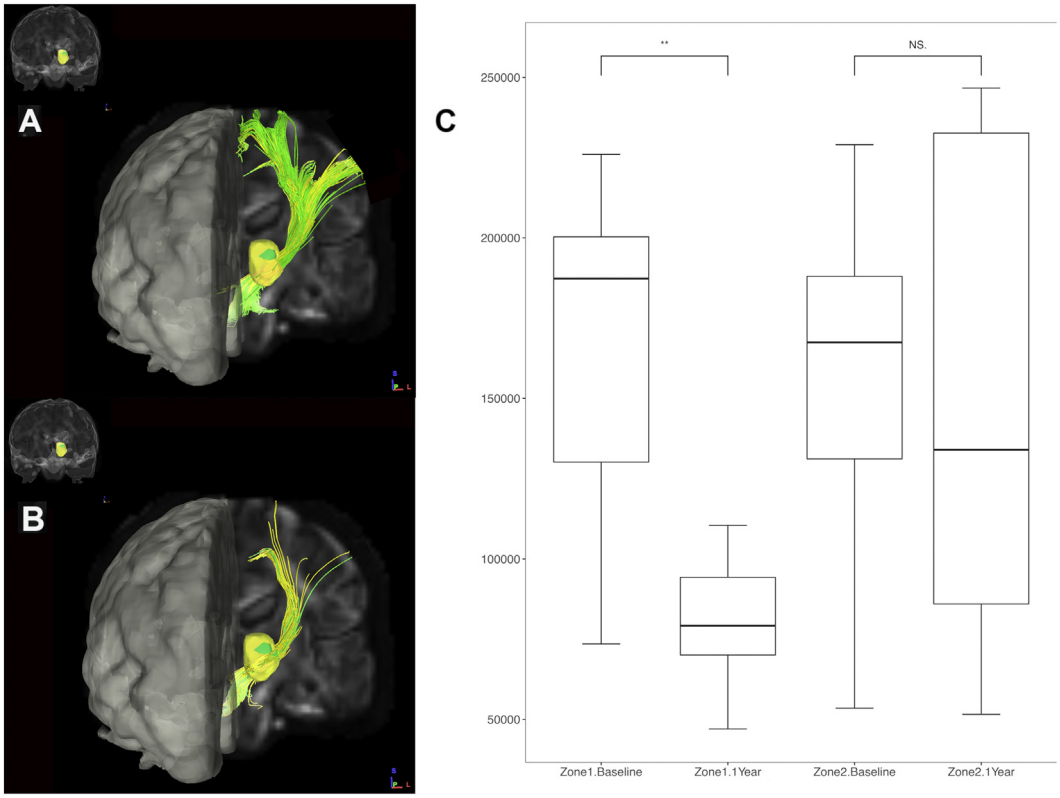

Fig. 5. Differences in streamline counts between zone 1 and zone 2 at 1 year (B) compared to pre-surgical baseline (A). Tractography using DSISTUDIO software for the nine patients with 1-year data; group template seeding from the group-level mask of zone 1 (green) and zone 2 (yellow). (C) Boxplots showing the number of streamlines per cluster and per time point. ** = t-test p-value < 0.001.

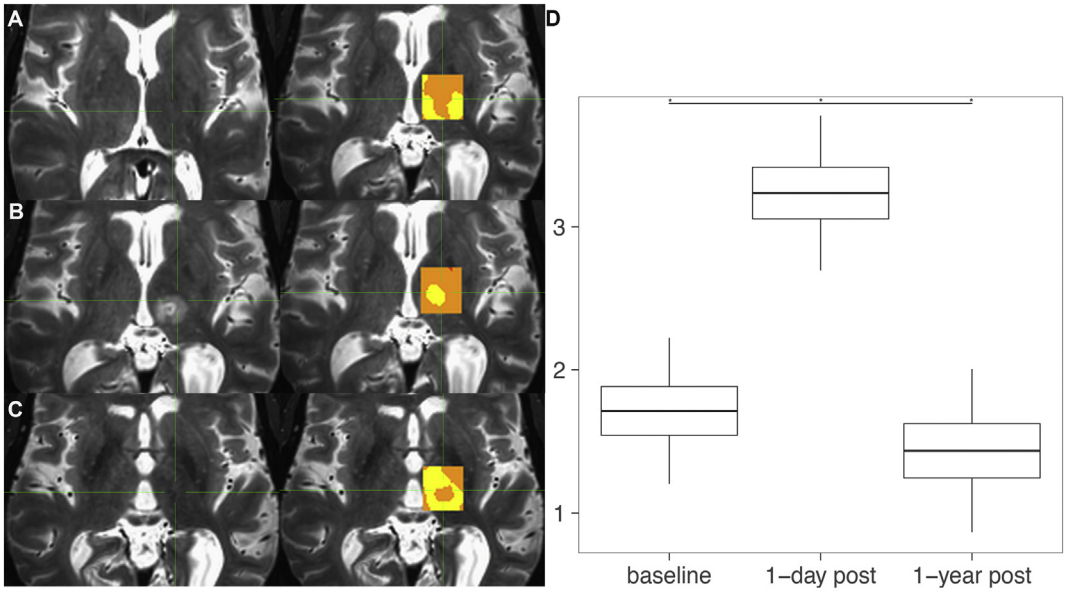

Fig. 6. Illustration of RDI changes at the single-patient level (ID 9 in Supplementary Table 1) between (A) baseline, (B) 1 day post imaging, and (C) 1 year post imaging. Right: RDI maps; Left: the corresponding T2 image. The median RDI values in zone 1, in this case, were 3.09 (SD 0.56) at 1 day post and 2.54 (SD 0.30) at 1 year post, while the values in the surrounding cluster were 2.20 (SD 0.32) and 1.36 (SD 0.28). (D) Bar graph showing the median RDI in zone 1 between baseline (left), 1 day post (middle), and 1 year post (right) at the group level. * = comparisons that are significant with $p < 0.01$.

Several groups have described the effects of high-frequency ultrasonic energy on the brain in animal models. Vykhodtseva et al. performed ultrasonic lesions in the brains of 13 rabbits in vivo, using a transducer capable of 1.5 MHz frequency (Vykhodtseva et al., 2001). The authors observed a consistent pattern on immediate histological examination, consisting of three different zones of tissue injuries, graded from coagulative necrosis to normal tissue. Another study, looking at the effects of the application of graded delivery of energy through FUS to ex-vivo rabbit brains, found a poor correlation between the area of coagulative necrosis and the peak temperature at the target (Hynynen et al., 2004). Currently, there are no reports in humans of histology after modern transcranial FUS-T. However, the behavior of

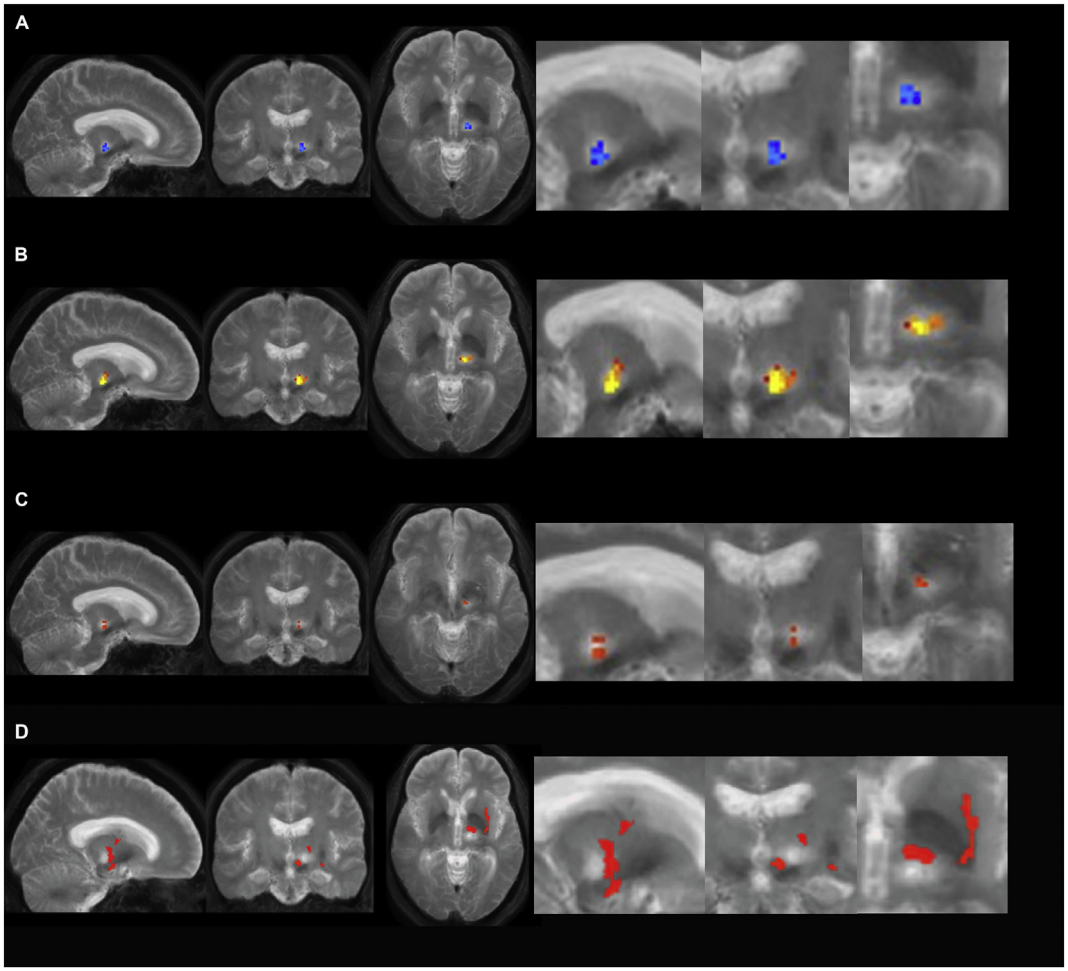

Fig. 7. Group-level comparison of RDI values. (A) Voxels with a significant increase in RDI at 1 day post-FUS-T across all patients (FSL randomise *t*-test, 18 comparisons, 5000 permutations with TFCE). (B) Voxels with significant RDI increase when accounting for tremor improvement at 3 months. (C) Voxels with significant RDI decrease at 1 year. (D) Surviving voxels after the *t*-test between 1 day post and 1 year post RDI images, after adjusting for percentage of tremor improvement.

focused ultrasound lesions in the thalamus appears, in some aspects, different from what is experienced using radiofrequency; e.g., the reported lesion size is bigger (Krishna et al., 2018a,b), lesions tend to disappear in the long term (Wintermark et al., 2014), and there is significant edema acutely after FUS-T. Previous reportd have contemplated the presence of three distinct 'zones' with different intensities on T2-weighted imaging (Harary et al., 2018a). However, the microstructural changes in the lesion area have not been studied in vivo using dMRI.

Based on the previously reported poor reliability of FA values in regions with higher free water contamination (Metzler-Baddeley et al., 2012), we decided to use the RDI metric for this analysis, which also accounts for free water contamination. Our results show that the area with an increase in RDI is represented by a volume largely overlapping with the lesion on T2-weighted imaging. When accounting for tremor improvement, however, the voxels with RDI increase are located around the lesion core and extending below thalamus. We also found that RDI values decreased at 1 year with the most marked decrease in zone 2, corresponding to the periphery of the lesion. When the group differences were adjusted for tremor improvement, we found that voxels in the subthalamic zone survived thresholding ($p < 0.05$). Previously, others have postulated that the substrate for tremor reduction after lesioning surgery may extend into the subthalamic area (Ashkan et al., 2007; Bergman et al., 1990). Similar findings have also been reported in the DBS literature, where targeting the posterior subthalamic zone was associated with good tremor reduction (Blomstedt et al., 2010; Sandvik et al., 2011). With the increased 'freedom' in performing FUS ablations in different locations without requiring additional 'brain passes' (as in the historical data), FUS technology can help us develop a better understanding of the optimal lesion parameters for sustained tremor reduction. In our previous analysis we did not identify a relationship between lesion size and tremor outcomes (Krishna et al., 2018a,b). However, the present analysis provides further insights in a larger cohort using the RDI metric. Our findings may support performing additional ablations in the ventral thalamus, especially anteriorly, toward the VIM/Vop border and medial to the VIM. Previous reports have confirmed the presence of tremor cells in this area during MER (Lenz et al., 1994). In addition, the involvement of the gray-white matter junction between the thalamus and subthalamic zone in the lesion area may be important for long-term tremor reduction.

5. Limitations

This is a prospective cohort study with a small cohort of patients. A single b-value cannot differentiate between different zones of restricted diffusion (more restricted vs. less restricted, or hindered diffusion). With advance multishell acquisition or diffusion spectrum imaging, RDI can be further used to quantify different zones of restricted diffusion.

Supplementary data to this article can be found online at https://

doi.org/10.1016/j.nicl.2019.101754.

Acknowledgments

We thank Ms. Reghan Borer for editing the manuscript.

Ethics statement

This work was carried out in accordance with The Code of Ethics of the World Medical Association (Declaration of Helsinki).

Declarations of interest

None.

Funding sources

None.

Author contributions

FS, VK: conception and design of the study, acquisition and analysis of data, drafting a significant portion of the manuscript or figures.
FY: drafting a significant portion of the manuscript or figures.

Funding sources

The support for this work was provided in part by the Discovery Themes Initiative and Neurological Research Institute, The Ohio State University. Some patients included in this analysis were treated using clinical trial funding from Insightec Inc.

Competing interests

The authors report no competing interests.

References

Ashkan, K., Blomstedt, P., Zrinzo, L., Tisch, S., Yousry, T., Limousin-Dowsey, P., Hariz, M., 2007. Variability of the subthalamic nucleus: the case for direct MRI guided targeting. Br. J. Neurosurg. 21, 197–200.
Avants, B.B., Tustison, N., Song, G., 2009. Advanced normalization tools (ANTS). Insight J. 2, 1–35.
Basser, P.J., 1995. Inferring microstructural features and the physiological state of tissues from diffusion-weighted images. NMR Biomed. 8, 333–344.
Bergman, H., Wichmann, T., DeLong, M.R., 1990. Reversal of experimental parkinsonism by lesions of the subthalamic nucleus. Science 249, 1436–1438.
Blomstedt, P., Sandvik, U., Tisch, S., 2010. Deep brain stimulation in the posterior subthalamic area in the treatment of essential tremor. Mov. Disord. 25, 1350–1356.
Boutet, A., Ranjan, M., Zhong, J., Germann, J., Xu, D., Schwartz, M.L., Lipsman, N., Hynynen, K., Devenyi, G.A., Chakravarty, M., Hlasny, E., Llinas, M., Lozano, C.S., Elias, G.J.B., Chan, J., Coblentz, A., Fasano, A., Kucharczyk, W., Hodaie, M., Lozano, A.M., 2018. Focused ultrasound thalamotomy location determines clinical benefits in patients with essential tremor. Brain 141, 3405–3414.
Burzynska, A.Z., Preuschhof, C., Bäckman, L., Nyberg, L., Li, S.-C., Lindenberger, U., Heekeren, H.R., 2010. Age-related differences in white matter microstructure: region-specific patterns of diffusivity. Neuroimage 49, 2104–2112.
Chang, J.W., Park, C.K., Lipsman, N., Schwartz, M.L., Ghanouni, P., Henderson, J.M., Gwinn, R., Witt, J., Tierney, T.S., Cosgrove, G.R., 2018. A prospective trial of magnetic resonance–guided focused ultrasound thalamotomy for essential tremor: results at the 2-year follow-up. Ann. Neurol. 83, 107–114.
Charrad, M., Ghazzali, N., Boiteau, V., Niknafs, A., Charrad, M.M., 2014. Package 'NbClust. J. Stat. Softw. 61, 1–36.
Chen, L., ter Haar, G., Hill, C.R., 1997. Influence of ablated tissue on the formation of high-intensity focused ultrasound lesions. Ultrasound Med. Biol. 23, 921–931.
Elias, W.J., Huss, D., Voss, T., Loomba, J., Khaled, M., Zadicario, E., Frysinger, R.C., Sperling, S.A., Wylie, S., Monteith, S.J., 2013a. A pilot study of focused ultrasound thalamotomy for essential tremor. N. Engl. J. Med. 369, 640–648.
Elias, W.J., Khaled, M., Hilliard, J.D., Aubry, J.-F., Frysinger, R.C., Sheehan, J.P., Wintermark, M., Lopes, M.B., 2013b. A magnetic resonance imaging, histological, and dose modeling comparison of focused ultrasound, radiofrequency, and gamma knife radiosurgery lesions in swine thalamus. J. Neurosurg. 119, 307–317.
Elias, W.J., Khaled, M., Hilliard, J.D., Aubry, J.F., Frysinger, R.C., Sheehan, J.P., Wintermark, M., Lopes, M.B., 2013c. A magnetic resonance imaging, histological, and dose modeling comparison of focused ultrasound, radiofrequency, and Gamma Knife radiosurgery lesions in swine thalamus. J. Neurosurg. 119 (2), 307–317.
Elias, W.J., Lipsman, N., Ondo, W.G., Ghanouni, P., Kim, Y.G., Lee, W., Schwartz, M., Hynynen, K., Lozano, A.M., Shah, B.B., 2016. A randomized trial of focused ultrasound thalamotomy for essential tremor. N. Engl. J. Med. 375, 730–739.
FDA, 2016. FDA Approves First MRI-Guided Focused Ultrasound Device to Treat Essential Tremor.
Fry, W.J., Mosberg Jr., W., Barnard, J., Fry, F., 1954. Production of focal destructive lesions in the central nervous system with ultrasound. J. Neurosurg. 11, 471–478.
Harary, M., Essayed, W.I., Valdes, P.A., McDannold, N., Cosgrove, G.R., 2018a. Volumetric analysis of magnetic resonance–guided focused ultrasound thalamotomy lesions. Neurosurg. Focus. 44, E6.
Harary, M., Segar, D.J., Huang, K.T., Tafel, I.J., Valdes, P.A., Cosgrove, G.R., 2018b. Focused ultrasound in neurosurgery: a historical perspective. Neurosurg. Focus. 44, E2.
Hariz, G.-M., Lindberg, M., Bergenheim, A.T., 2002. Impact of thalamic deep brain stimulation on disability and health-related quality of life in patients with essential tremor. J. Neurol. Neurosurg. Psychiatry 72, 47–52.
Hirai, T., Miyazaki, M., Nakajima, H., Shibazaki, T., Ohye, C., 1983. The correlation between tremor characteristics and the predicted volume of effective lesions in stereotaxic nucleus ventralis intermedius thalamotomy. Brain 106, 1001–1018.
Hynynen, K., Clement, G.T., McDannold, N., Vykhodtseva, N., King, R., White, P.J., Vitek, S., Jolesz, F.A., 2004. 500-element ultrasound phased array system for noninvasive focal surgery of the brain: a preliminary rabbit study with ex vivo human skulls. Magn. Reson. Med. 52, 100–107.
Ito, M., Watanabe, H., Kawai, Y., Atsuta, N., Tanaka, F., Naganawa, S., Fukatsu, H., Sobue, G., 2007. Usefulness of combined fractional anisotropy and apparent diffusion coefficient values for detection of involvement in multiple system atrophy. J. Neurol. Neurosurg. Psychiatry 78, 722–728.
Jenkinson, M., Beckmann, C.F., Behrens, T.E., Woolrich, M.W., Smith, S.M., 2012. Fsl. Neuroimage 62, 782–790.
Kennedy, J., Ter Haar, G., Cranston, D., 2003. High intensity focused ultrasound: surgery of the future? Br. J. Radiol. 76, 590–599.
Krishna, V., Sammartino, F., Agrawal, P., Changizi, B.K., Bourekas, E., Knopp, M.V., Rezai, A., 2018a. Prospective tractography-based targeting for improved safety of focused ultrasound thalamotomy. Neurosurgery 84 (1), 160–168.
Krishna, V., Sammartino, F., Rezai, A., 2018b. A review of the current therapies, challenges, and future directions of transcranial focused ultrasound technology: advances in diagnosis and treatment. JAMA Neurol. 75, 246–254.
Lenz, F., Kwan, H., Martin, R., Tasker, R., Dostrovsky, J., Lenz, Y., 1994. Single unit analysis of the human ventral thalamic nuclear group: tremor-related activity in functionally identified cells. Brain 117, 531–543.
Metzler-Baddeley, C., O'Sullivan, M.J., Bells, S., Pasternak, O., Jones, D.K., 2012. How and how not to correct for CSF-contamination in diffusion MRI. Neuroimage 59, 1394–1403.
Pasternak, O., Westin, C.-F., Bouix, S., Seidman, L.J., Goldstein, J.M., Woo, T.-U.W., Petryshen, T.L., Mesholam-Gately, R.I., McCarley, R.W., Kikinis, R., 2012. Excessive extracellular volume reveals a neurodegenerative pattern in schizophrenia onset. J. Neurosci. 32, 17365–17372.
Pierpaoli, C., Walker, L., Irfanoglu, M., Barnett, A., Basser, P., Chang, L., Koay, C., Pajevic, S., Rohde, G., Sarlls, J., 2010. TORTOISE: An Integrated Software Package for Processing of Diffusion MRI Data. Book TORTOISE: An Integrated Software Package for Processing of Diffusion MRI Data (Editor Edˆ Eds) 18, 1597.
Robin, X., Turck, N., Hainard, A., Tiberti, N., Lisacek, F., Sanchez, J.-C., Müller, M., 2011. pROC: an open-source package for R and S+ to analyze and compare ROC curves. BMC Bioinforma. 12, 77.
Rohde, G.K., Barnett, A.S., Basser, P.J., Marenco, S., Pierpaoli, C., 2004. Comprehensive approach for correction of motion and distortion in diffusion-weighted MRI. Magn. Reson. Med. 51, 103–114.
Saad, Z.S., Reynolds, R.C., Argall, B., Japee, S., Cox, R.W., 2004. SUMA: an interface for surface-based intra-and inter-subject analysis with AFNI. Biomedical Imaging: Nano to Macro, 2004. In: IEEE International Symposium on. IEEE, pp. 1510–1513.
Sammartino, F., Krishna, V., King, N.K.K., Lozano, A.M., Schwartz, M.L., Huang, Y., Hodaie, M., 2016. Tractography-based ventral intermediate nucleus targeting: novel methodology and intraoperative validation. Mov. Disord. 31, 1217–1225.
Sandvik, U., Koskinen, L.-O., Lundquist, A., Blomstedt, P., 2011. Thalamic and subthalamic deep brain stimulation for essential tremor: where is the optimal target? Neurosurgery 70, 840–846.
Schuurman, P.R., Bosch, D.A., Bossuyt, P.M., Bonsel, G.J., Van Someren, E.J., De Bie, R.M., Merkus, M.P., Speelman, J.D., 2000. A comparison of continuous thalamic stimulation and thalamotomy for suppression of severe tremor. N. Engl. J. Med. 342, 461–468.
Smith, S.M., Nichols, T.E., 2009. Threshold-free cluster enhancement: addressing problems of smoothing, threshold dependence and localisation in cluster inference. Neuroimage 44, 83–98.
Vykhodtseva, N., Mcdannold, N., Martin, H., Bronson, R.T., Hynynen, K., 2001. Apoptosis in ultrasound-produced threshold lesions in the rabbit brain. Ultrasound Med. Biol. 27, 111–117.
Wintermark, M., Druzgal, J., Huss, D., Khaled, M., Monteith, S., Raghavan, P., Huerta, T., Schweickert, L., Burkholder, B., Loomba, J., 2014. Imaging findings in MR imaging–guided focused ultrasound treatment for patients with essential tremor. Am. J. Neuroradiol. 35, 891–896.
Yeh, F.C., Tseng, W.Y., 2011. NTU-90: a high angular resolution brain atlas constructed by q-space diffeomorphic reconstruction. Neuroimage 58, 91–99.
Yeh, F.-C., Wedeen, V.J., Tseng, W.-Y.I., 2010. Generalized ${q} $-sampling imaging. IEEE Trans. Med. Imaging 29, 1626–1635.
Yeh, F.C., Liu, L., Hitchens, T.K., Wu, Y.L., 2017. Mapping immune cell infiltration using restricted diffusion MRI. Magn. Reson. Med. 77, 603–612.
Zhang, H., Wang, Y., Lu, T., Qiu, B., Tang, Y., Ou, S., Tie, X., Sun, C., Xu, K., Wang, Y., 2013. Differences between generalized q-sampling imaging and diffusion tensor imaging in the preoperative visualization of the nerve fiber tracts within peritumoral edema in brain. Neurosurgery 73, 1044–1053.